Journal of Wind Engineering & Industrial Aerodynamics 172 (2018) 325–340

Contents lists available at ScienceDirect

Journal of Wind Engineering & Industrial Aerodynamics

journal homepage: www.elsevier.com/locate/jweia

A statistical dynamics track model of tropical cyclones for assessing typhoon wind hazard in the coast of southeast China

Yu Chen, Zhongdong Duan *

Department of Civil and Environmental Engineering, Harbin Institute of Technology, Shenzhen Graduate School, Shenzhen, China

ARTICLE INFO

Keywords:
Track model
Statistical dynamics
Typhoon wind hazard
Monte Carlo method

ABSTRACT

An improved full track model for tropical cyclones (TCs) based on statistical dynamics method is developed to estimate typhoon wind hazard in the coast of southeast China. The track model includes genesis model, movement model, and intensity model. The genesis model is established based upon an improved kernel probability density function with the biased cross-validation bandwidth. The movement model is developed based on the Beta and Advection Model (BAM). The intensity model consists of an auto-regression ocean intensity model and an inland decay model using the nearest neighbor method. Using the historical environment data, 1000 years TC tracks are simulated by the improved model and compared with features of the historical tracks in the western North Pacific (WNP) basin, the results verify that the developed model performs well. Moreover, typhoon wind hazard in the coastal areas of southeast China is estimated by the improved track model combined with a parametric wind field model. Compared with the current Chinese design code, the relative differences between estimated return period velocities and those recommended in design code are less than 13.4%. The developed model enables analyzing typhoon hazard in the context of climate change, which is our future task.

1. Introduction

Tropical cyclone (TC) is a devastating natural disaster which produces strong wind, storm surge, and heavy rainfall. It accounts for the majority of natural catastrophic losses in the developed world and, next to floods, is the leading cause of death and injury among natural disasters affecting developing countries (Emanuel et al., 2008). The western North Pacific (WNP) basin is the area most affected by TCs, thus the wind resistance design and regional insurance industry need to assess the risk of TCs in order to reduce the losses caused by TCs. Nevertheless, the historical TC records are limited and the quality of historical records cannot be guaranteed due to the loss of records and inaccuracy of observation apparatuses. Consequently, it's of interest to develop a method for extending TC data.

A traditional method of expanding TC dataset is the single site probabilistic model proposed by Russell (1971), followed by the development of Tryggvason et al. (1976), Batts et al. (1980), Georgiou (1985), Vickery and Twisdale (1995). The basic idea of this method is to form a region by expanding a defined radius from a single site (radius is generally 200–300 km), and then analyzes the statistical characteristics of historical TCs which pass through this region. According to the statistical features, a large number of TCs can be synthesized through the Monte Carlo method to expand typhoon regional dataset for wind hazard analyses. This method is mature to the small areas while cumbersome to perform for hazard analyses in large areas, such as coastal multi-cities, railways, and power grid systems. Moreover, the single site model is deficient in the high latitude regions with insufficient historical records.

To estimate the risk of TCs in a larger area, an empirical full track model utilizing statistical characteristics of historical track records directly is proposed to synthesize a large number of full tracks over the whole ocean (Vickery et al., 2000; James and Mason, 2005; Hall and Jewson, 2007). The empirical track model can be divided into three parts: genesis model, movement model, and intensity model. As the synthetic track model segments the life of TCs and the physical significance of each segment is clear, it is possible to assess TC hazard in a wider area. Likewise, this empirical track model relies too much on historical track data, thus it performs well in TC-rich areas, but underperforms in regions where historical records are rare. Recently, a track model based on statistical dynamics method has been proposed to overcome this shortcoming (Emanuel et al., 2006; Vickery et al., 2010). Unlike the empirical track model, the statistical dynamics relationship of TC motion is developed rather than simply statistical characteristics of historical tracks, and then combined with the environment data which cover the whole world for synthesizing full tracks. Therefore the synthetic full track

* Corresponding author.
E-mail address: duanzd@hit.edu.cn (Z. Duan).

https://doi.org/10.1016/j.jweia.2017.11.014
Received 13 May 2017; Received in revised form 15 November 2017; Accepted 15 November 2017
Available online 25 November 2017
0167-6105/© 2017 Elsevier Ltd. All rights reserved.

model can be applied to historical records scarce areas where we have an interest in assessing TC risk. In addition, since the statistical dynamics relationship of each part in the model is well defined, the statistical dynamics track model can be combined with variable climatic environmental data to assess TC activities under the context of climate change (Colbert et al., 2013; Emanuel, 2013).

This paper further improves the genesis and movement model and establishes a new intensity regression model for estimating typhoon wind hazard in the coast of southeast China. For the genesis positions, the genesis model is improved based upon a revised kernel probability density function with the biased cross-validation best bandwidth to avoid the genesis probability for lands. For the movements, the 6-h translational velocity is divided into steering velocity and beta-drift velocity; the former is defined as annulus pressure-weighted mean wind velocity and the latter is estimated by regional mean beta-drift velocity. Moreover, a lag-two autoregressive method based on maximum wind speed is used to establish the ocean intensity model with new regression variables selected by stepwise regression method. The inland decay model is fitted as a decreasing function through selecting the k nearest landing positions. A large number of full tracks are simulated using the historical environment data and compared with features of the historical tracks in the WNP basin. Finally, the improved statistical dynamics track model combined with a parametric wind field model is given to estimate typhoon wind risk in the coastal areas of the southeast China.

2. Data

The data used in this improved track model are shown as following. The Joint Typhoon Warning Center (JTWC) best-track dataset is used to represent the observed TC events, which include 1951 historical TCs for a total of 70 years from 1945 to 2014. The target area of JTWC is the WNP basin (including the South China Sea), the statistical data include every 6 h of center location, maximum sustained wind speed, central minimum pressure, maximum wind speed radius, and radius of specified wind intensity. It is noteworthy that JTWC started providing data to the last three parameters since 2001. It is assumed that inland cannot generate TCs, so all records whose initial positions locate in the inland are deleted from the dataset.

Atmospheric and oceanic environment parameters include monthly mean sea surface temperature, 4 times daily environmental wind velocity, monthly mean atmospheric ambient temperature, and monthly mean atmospheric ambient specific humidity. In these parameters, except that the sea surface temperature is obtained from the COBE-SST dataset which provides a resolution of 1° in both latitude and longitude (Ishii et al., 2005), the rest of the parameters are from the National Centers for Environmental Prediction-National Center for Atmospheric Research (NCEP-NCAR) reanalysis dataset which provides a resolution of 2.5° in both directions (Kalnay et al., 1996). The environmental wind velocity and atmospheric ambient temperature in the NCEP-NCAR reanalysis dataset have 17 vertical levels from 1000 hpa to 10 hpa while the specific humidity is only available for the lowest 8 levels. Therefore, the specific humidity of the rest levels is assumed to zero due to extremely small value. All environment parameters are interpolated into TC center locations and time in simulation process.

3. Statistical dynamics track model development

The basic simulation procedures for synthesizing full tracks are similar to Vickery et al. (2000). First of all, the genesis model generates annual occurrence numbers and initial positions (including latitude, longitude and time). Secondly, the movement model simulates the translational speeds to propagate TCs to the next positions along minimum arc between two positions on the earth in 6 h. The subsequent locations are then continually updated with similar procedures. Meanwhile, intensity model estimates the TC intensity at each position. Finally, the full track model is terminated when the simulated intensity is lower than tropical depression. Although the improved statistical dynamics model inherits the idea of synthetic full track, it distinguishes it from Vickery's empirical full track model. This model is improved in the genesis, track and intensity simulation of TCs based on a more solid meteorological basis. The following subsections focus on the improvements for full track model in detail.

3.1. Genesis model

Unlike the traditional method which extracts directly historical genesis positions and performs parameter estimation for annual genesis numbers (Vickery et al., 2000; Li and Hong, 2016), here, a nonparametric method is adopted to simulate annual genesis numbers and initial positions. The nonparametric method doesn't require a prior distribution hypothesis, relying entirely on the training data. Therefore, this method is simple and intuitive, and easy to understand. As a matter of fact, Terrell and Scott (1992) have rigorously demonstrated that almost all nonparametric methods are asymptotic kernel density methods. The kernel probability density basic functions are as follows.

$$f(\boldsymbol{x}) = \frac{1}{nh}\sum_{i=1}^{n} K\left(\frac{\boldsymbol{x}-\boldsymbol{x}_i}{h}\right) \tag{1}$$

where $\boldsymbol{x}$ is the vector to be estimated; $\boldsymbol{x}_i$ is the ith sample vector; h is the bandwidth; n is the sample size; $K(\bullet)$ is the kernel density estimator, and the Gaussian kernel density function is used in this paper. First, Eq. (1) is employed to estimate the probability density of annual occurrence number in the WNP basin. Choosing an appropriate bandwidth is a key to accurately estimate the kernel probability density, because too large or too small bandwidth will cause the estimated probability density too smooth or too rough respectively.

Here, a one-dimensional Gaussian kernel biased cross-validation method proposed by Scott (2012) is used to calculate the optimal bandwidth of the annual occurrence number probability density as shown below.

$$BCV(h) = \frac{1}{2nh\sqrt{\pi}} + \frac{1}{64n^2h\sqrt{n}}\cdot\sum_{i<j}\left(\Delta_{ij}^4 - 12\Delta_{ij}^2 + 12\right)\exp\left(-\Delta_{ij}^2/4\right) \tag{2}$$

where $\Delta_{ij}=(x_i-x_j)/h$, x_i and x_j represent the ith and jth annual sample number of TCs respectively. Using the JTWC 70-year best-track dataset, the optimal bandwidth h is obtained by minimizing Eq. (2). By substituting the optimal bandwidth into Eq. (3), the probability density of annual occurrence number can be estimated easily.

$$\widehat{f}(x) = \frac{1}{70h}\sum_{i=1}^{70}\frac{1}{\sqrt{2\pi}}\exp\left(-\frac{(x-x_i)^2}{2h^2}\right) \tag{3}$$

Since the annual occurrence number of TCs is discrete, it is necessary to integrate the estimated probability density to obtain the discrete probability of the annual number. Finally, a large number of annual occurrence numbers of TCs are simulated by Monte Carlo method. In order to further inspect whether the distribution of simulated annual occurrence number is consistent with historical distribution, two nonparametric tests, Kolmogorov-Smirnov test and rank sum test, are used to verify the consistency of distribution with a significant level of 0.05. The results of both two nonparametric tests demonstrate the consistency of distribution.

Likewise a three-dimensional kernel density function is used to estimate the space-time probability density of TC genesis position. The space-time of TC genesis position is composed of three dimensions: latitude, longitude and time. Since the simulated TC generation positions are periodic in time dimension with a period 0–366 days, it is necessary to extend the historical generation positions to 3 times in the time dimension for considering the impact the last year and next year genesis

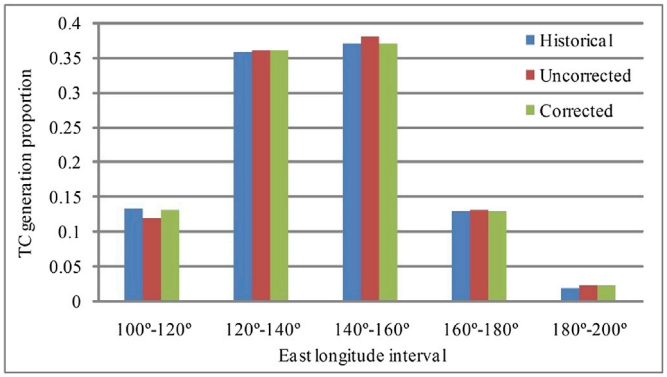

Fig. 1. TC generation proportions within east longitude intervals of 20°.

positions on the probability densities of genesis positions at this year. As the three dimensions have different quantities and units, the historical samples should be normalized by using Eq. (4) so as to avoid one or more dimensions dominate the others in kernel density estimation.

$$\boldsymbol{z}_i = \boldsymbol{S}^{-1}(\boldsymbol{x}_i - \boldsymbol{m}) \tag{4}$$

where $\boldsymbol{m}$ and $\boldsymbol{S}$ are the mean vector and standard deviation matrix of the TC genesis position, respectively; $\boldsymbol{x}_i$ is the ith sample of the genesis position. The principal component analysis is used to transform the three related dimensions of normalized samples to unrelated ones. After above conversion, the transformed samples are substituted into a three-dimensional product kernel density function to estimate the probability density of genesis position. The optimum bandwidths of three-dimensional product kernel density function are calculated by minimizing Eq. (5) using a three-dimensional biased cross-validation method (Sain et al., 1994). This optimum bandwidth enables the estimated probability of the result closer to a reasonable value meanwhile the calculation speed can be faster.

$$\begin{aligned} BCV(h_1,h_2,h_3) = {} & \frac{1}{(2\sqrt{\pi})^3 n h_1 h_2 h_3} \\ & + \frac{1}{4n(n-1)h_1 h_2 h_3} \\ & \cdot \sum_{i=1}^{n} \sum_{j \neq i} \left[\left(\Delta_{ij1}^2 + \Delta_{ij2}^2 + \Delta_{ij3}^2 \right)^2 \right. \\ & \left. - 10\left(\Delta_{ij1}^2 + \Delta_{ij2}^2 + \Delta_{ij3}^2 \right) + 15 \right] \\ & \cdot \left[\frac{1}{2\pi\sqrt{2\pi}} \exp\left(- \frac{\Delta_{ij1}^2 + \Delta_{ij2}^2 + \Delta_{ij3}^2}{2} \right) \right] \end{aligned} \tag{5}$$

where $\Delta_{ijk}=(x_{ik}-x_{jk})/h_k$, x_{ik} and x_{jk} represent the kth dimension of the ith and jth normalized variables, h_k represents the kth dimensional bandwidth, $k = 1, 2, 3$.

Unfortunately, the three-dimensional kernel density estimator distributes some of the genesis probabilities to lands, which obviously contradicts to the physical conditions of TCs. If the inland generation probability is simply deleted, the estimated genesis probability of sea near the adjacent lands would be relatively lower. As shown in Fig. 1, the TC generation proportion from 100° to 120° east longitude estimated by the uncorrected kernel density function is 11.7% lower than the

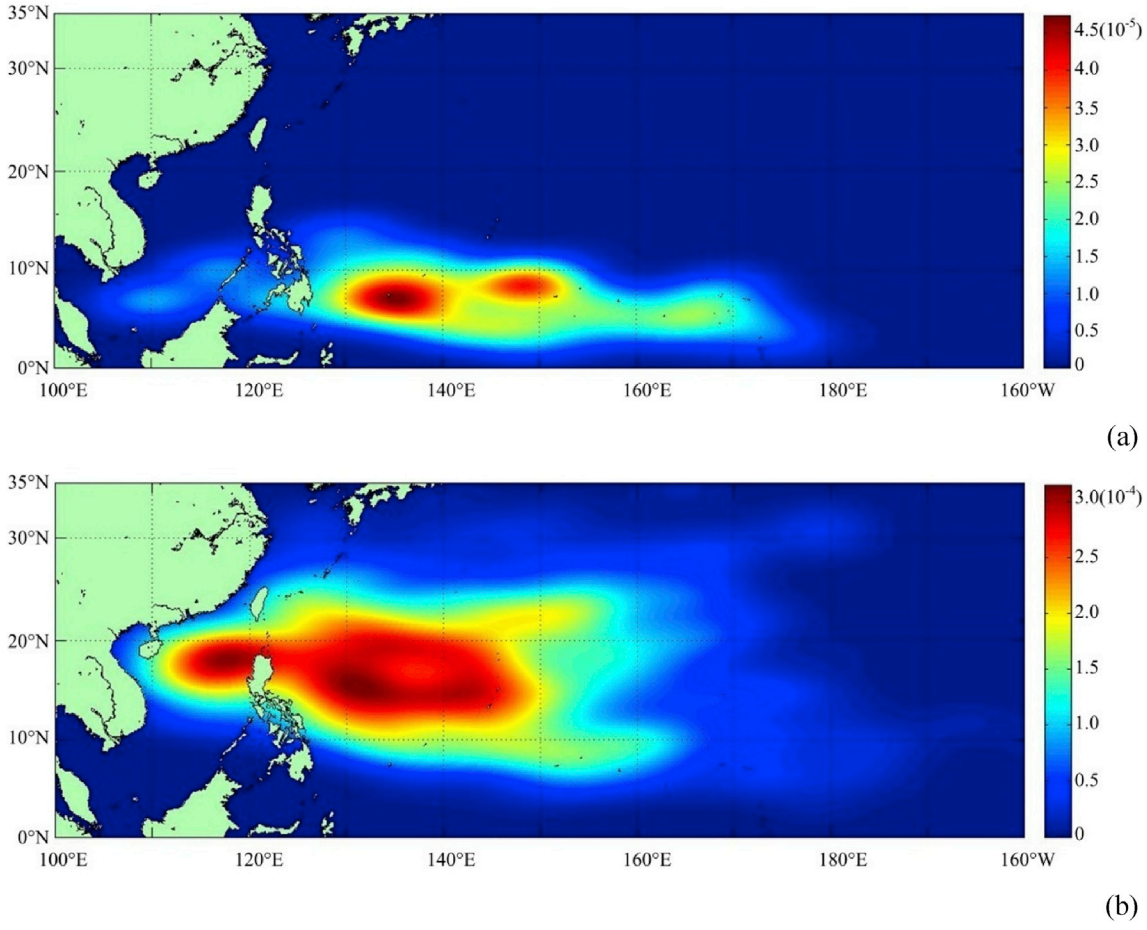

Fig. 2. Estimated probability density distribution of TC genesis location in February (a) and August (b).

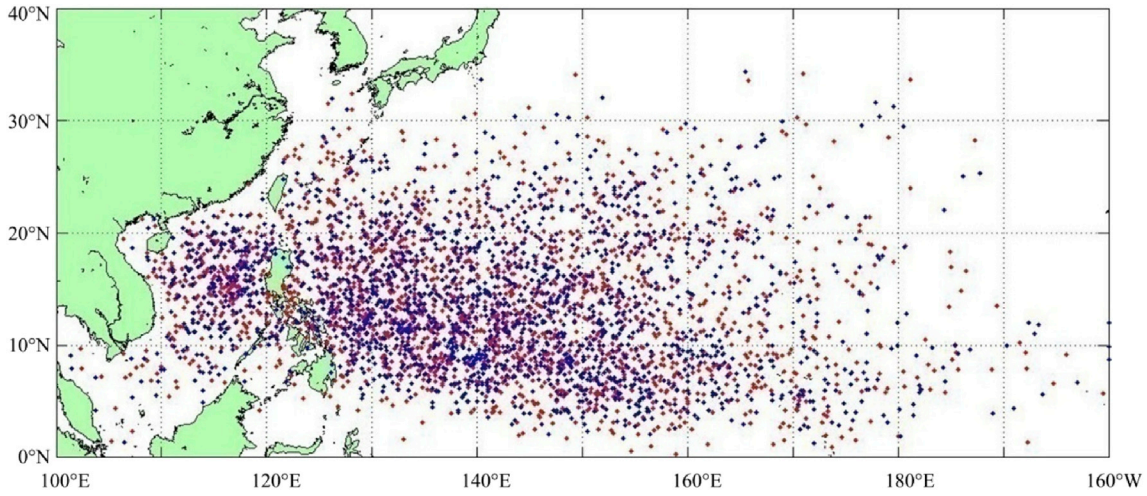

Fig. 3. Simulated genesis positions (red points) and history genesis positions (blue points). (For interpretation of the references to colour in this figure legend, the reader is referred to the web version of this article.)

historical statistic, which seriously underestimates the generation proportion in the South China Sea. The main reason for the low estimation is that this longitude range contains a lot of lands. Therefore it is necessary to revise the estimated generation probability of sea near the adjacent lands.

In this paper, the inland generation probability estimated by each kernel density estimator is assigned back to the estimator itself for revising the estimated generation probability of sea near the adjacent lands. The finally revised probability density of generation position is shown in Eq. (6).

$$\widehat{f}(\boldsymbol{x}) = \frac{1}{(2\pi)^{\frac{3}{2}} n h_{opt1} h_{opt2} h_{opt3} \sqrt{\lambda_1\lambda_2\lambda_3\sigma_{xx}\sigma_{yy}\sigma_{zz}}} \cdot \sum_{i=1}^{n} w_i \exp\left\{ - \frac{\left[(\boldsymbol{\gamma}_1)^{\mathrm{T}} \boldsymbol{S}^{-1}(\boldsymbol{x}-\boldsymbol{x}_i)\right]^2}{2h_{opt1}^2\lambda_1} - \frac{\left[(\boldsymbol{\gamma}_2)^{\mathrm{T}} \boldsymbol{S}^{-1}(\boldsymbol{x}-\boldsymbol{x}_i)\right]^2}{2h_{opt2}^2\lambda_2} - \frac{\left[(\boldsymbol{\gamma}_3)^{\mathrm{T}} \boldsymbol{S}^{-1}(\boldsymbol{x}-\boldsymbol{x}_i)\right]^2}{2h_{opt3}^2\lambda_3} \right\} \tag{6}$$

where h_{opt1}, h_{opt2} and h_{opt3} are the optimal bandwidths; σ_{xx}, σ_{yy} and σ_{zz} are the variances of three dimensions (longitude, latitude and time); w_i is the revised weight of the ith kernel density estimator; γ_1, γ_2 and γ_3 are the eigenvectors of the correlation coefficients between the three normalized variables; λ_1, λ_2, λ_3 are eigenvalues. It can be seen from Fig. 1 that the proportions of TC genesis in the longitude intervals estimated by the revised kernel density function are much closer to the historical statistics than the uncorrected ones, the relative error in the interval of 100°–120° east longitude is only 0.98%.

The probability density distributions of TC generation locations are estimated by integrating Eq. (6) in time, and Fig. 2 shows the results of February and August for examples. As shown in Fig. 2, for the same location, there is significantly different generation probability at different months. Taking the South China Sea as an example, the TCs occur at low latitude in February and shift northward to the northern part of WNP in August, come into being one of the most densely populated areas affected by TCs. The TC genesis positions change with different seasons, so it is necessary to consider the effect of time on the generation positions.

Finally, a great quantity of initial positions is sampled from the estimated space-time probability density distribution of TC genesis position through Monte Carlo method. Fig. 3 shows the comparison between historical generation positions and simulated generation positions for 70 years. It can be seen that the distribution of the historical generation position is similar to that of the simulated one in general. Similarly, a chi-square goodness test is used to test the consistency of the two distributions, thus the domain in Fig. 3 are divided into 5° × 5° grids while the grids with less than 5 historical genesis positions are removed. The chi-square estimator sum (32.37) of total grids is less than chi-square threshold (89.39) at 5% significant level, indicating that their consistency is statistically significant at 95% confidence level.

3.2. Movement model

In this subsection, a statistical dynamics movement model, which is based on the Beta and Advection Model (BAM) rather than merely statistical characteristics of historical tracks, is used to simulate synthetic tracks of TCs. The statistical dynamics movement model combines the statistical and dynamical approaches based on a relationship between the TC movement behavior and atmospheric environmental variables. The BAM follows a trajectory in the pressure-weighted vertically-averaged horizontal wind from the Aviation model beginning at the current storm location, with a correction that accounts for the beta effect (Marks, 1992). Our trajectory model is similar to the BAM, where the TC movements are simulated based on large-scale environmental wind velocities obtained from the NCEP-NCAR reanalysis wind field of the period 1949–2014, and correction velocities estimated by the regional mean beta-drifts. This model can be not only applied to the historical records scarce areas but also the scenarios where climate environment changes. The translational velocity of TCs in each 6-h position is shown in Eq. (7) as following.

$$U = U_{steer} + B_x$$

$$V = V_{steer} + B_y \tag{7}$$

where U and V are the latitudinal and longitudinal velocity of TC movement, respectively; U_{steer} and V_{steer} are the latitudinal and longitudinal velocity of steering flow, respectively; B_x and B_y are the latitudinal and longitudinal term of beta drift, respectively.

In general, the steering flow is defined as a pressure weighted vertically-averaged horizontal wind over a proper annulus band. In the following sections, the TC steering flow is defined the same as Carr and Elsberry (1990), who recommends a 300 to 850 hpa pressure-weighted mean wind. Somewhat different from them, the average annulus band is defined as a radius of 5° latitude here instead of 5°–7°, because the overall average simulated track using vertically-averaged horizontal

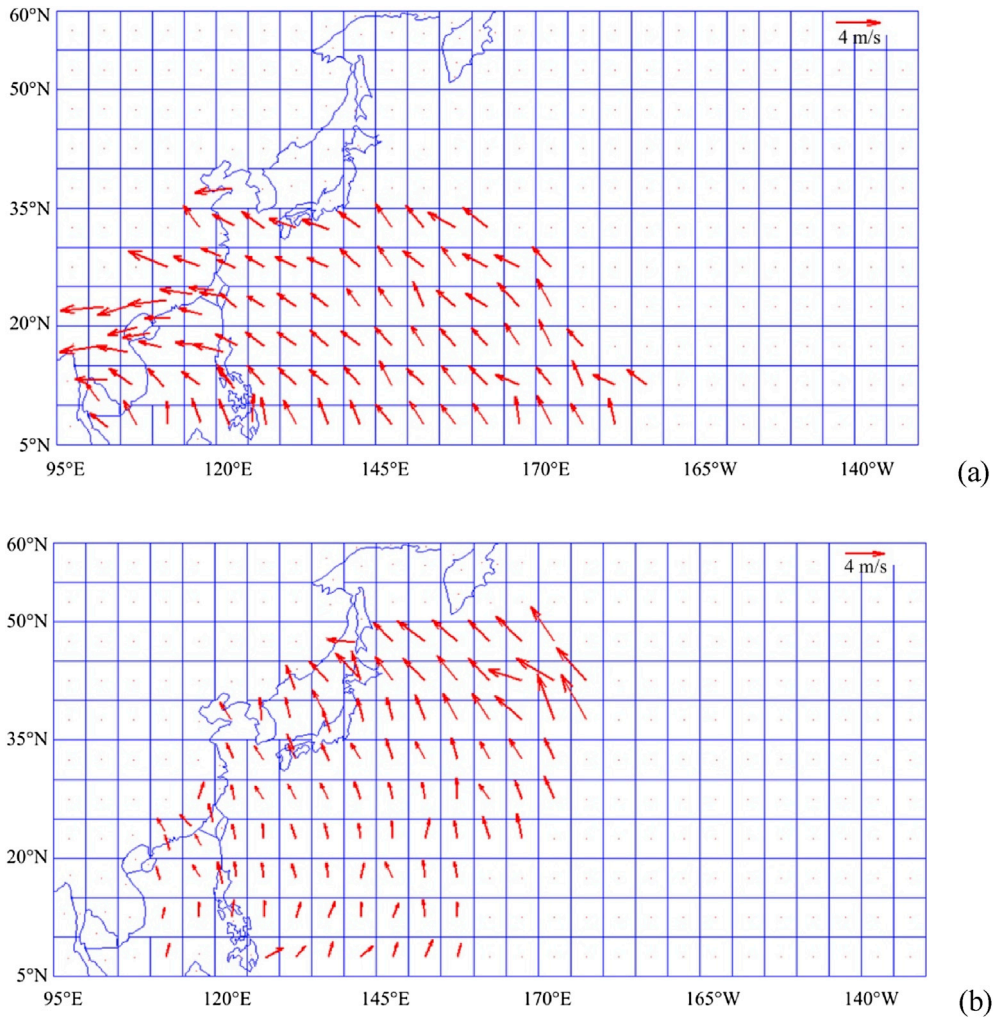

Fig. 4. Regional mean beta-drift velocities of TCs moving easterly (a) and westerly (b) in grids with more than 30 historical 6-h records.

wind over 5° annulus band is the most in accordance with the overall average historical track. The latitudinal and longitudinal velocities of steering flow are shown in Eq. (8) as following.

$$U_{steer} = \frac{1}{550}(50U_{300} + 100U_{400} + 100U_{500} + 100U_{600} + 125U_{700} + 75U_{850})$$

$$V_{steer} = \frac{1}{550}(50V_{300} + 100V_{400} + 100V_{500} + 100V_{600} + 125V_{700} + 75V_{850}) \quad (8)$$

where U_{300}, U_{400}, etc., are the latitudinal velocities of each pressure layer azimuthally averaged at a radius of 5° latitude; V_{300}, V_{400}, etc., are the longitudinal velocities of each pressure layer azimuthally averaged at a radius of 5° latitude.

The beta drift is an additional movement caused by the interaction of TCs with the environmental wind fields. Marks (1992) experimented with empirical magnitude range from 1 to 3 m/s and angle range from 295° to 315°. However, the complicated physical mechanism of the beta drift has not been fully explained yet (Chan, 2005). As there is no analytical solution for the beta drift, the regional mean beta-drift velocity is used as the beta drift term in Eq. (7). With the above defined steering velocity removed from historical 6-h translational velocity, the isolated beta drift is used to estimate the regional mean beta-drift velocity in each grid that historical TCs pass across. As illustrated in Fig. 4, areas with the same TC climatology are divided into cells, and all islands are isolated as individual cells. The remaining regions are divided into uniform 5°×5° grids. The overall average magnitude and direction for beta-drift velocity in WNP are 2.86 m/s and 310° respectively, which are in agreement with the Marks (1992). Moreover, the regional mean beta-drift velocities are obtained separately for easterly and westerly headed TCs as shown in Fig. 4 (a) and (b). The significant difference between the two regional mean beta-drift velocities can be seen from Fig. 4. The regional mean beta-drift velocities of TCs moving westerly on the ocean are usually northwestward, as shown in Fig. 4 (a), but the mean beta-drift velocities on the land gradually tend to the south. In contrast, the regional mean beta-drift velocities of TCs moving easterly are northeastward at lower latitude as shown in Fig. 4 (b), but veer to the northwest and become faster at higher latitude. It is should be noted that the regional mean beta-drift velocities are obtained in the neighborhood grids in the case of grids with less than 30 historical 6-h records. Using the NCEP-NCAR 4-times daily environmental wind field, the next 6-h position is determined through the translational velocity along minimum arc between the two positions on the earth in 6 h.

3.3. Intensity model

The statistical intensity model is used to estimate the TC intensity in every 6-h position for assessing typhoon wind hazard. The intensity model consists of an ocean intensity model and an inland decay model. While the simulated TCs move over the ocean, the ocean intensity model

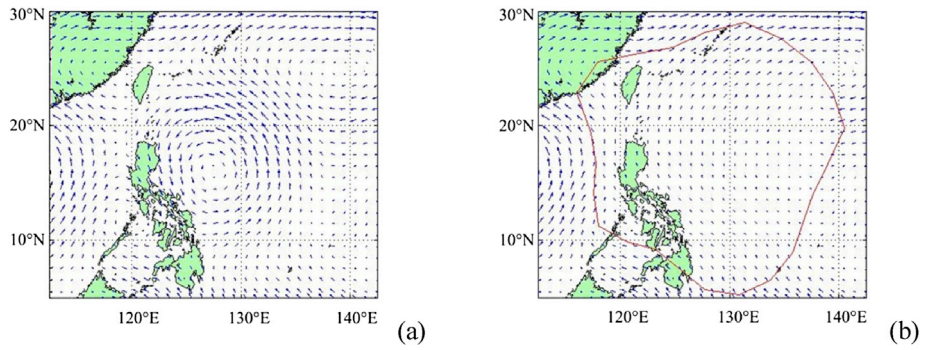

Fig. 5. 850 hPa layer original wind field of typhoon Nuri at 0000UTC/19/08/2008 (a) and 850 hPa layer environmental wind field of typhoon Nuri at 0000UTC/19/08/2008 (b). The red solid line is the boundary of removed analyzed vortex domain. (For interpretation of the references to colour in this figure legend, the reader is referred to the web version of this article.)

is adopted to estimate the intensities. In this paper, an autoregressive function is developed to establish the ocean intensity model. The change in the logarithm of relative intensity is used as the dependent variable, while the alternative independent variables consist of climatology and persistence variables, and atmospheric and oceanic environmental parameters, such as the maximum wind velocity, the potential intensity, the relative intensity, the sea surface temperature, and the vertical wind shear between 850 hpa and 200 hpa. Moreover, the changes of those variables in 6-h are also included as independent variables. Using the stepwise regression method, the independent variables are selected from the alternative independent variables. A lag-one autoregressive equation of the ocean intensity is used for estimating the intensity at second position, as shown in Eq. (9a), for which the R-squared is 0.295 in the WNP basin. For the intensities of third and subsequent positions, a lag-two

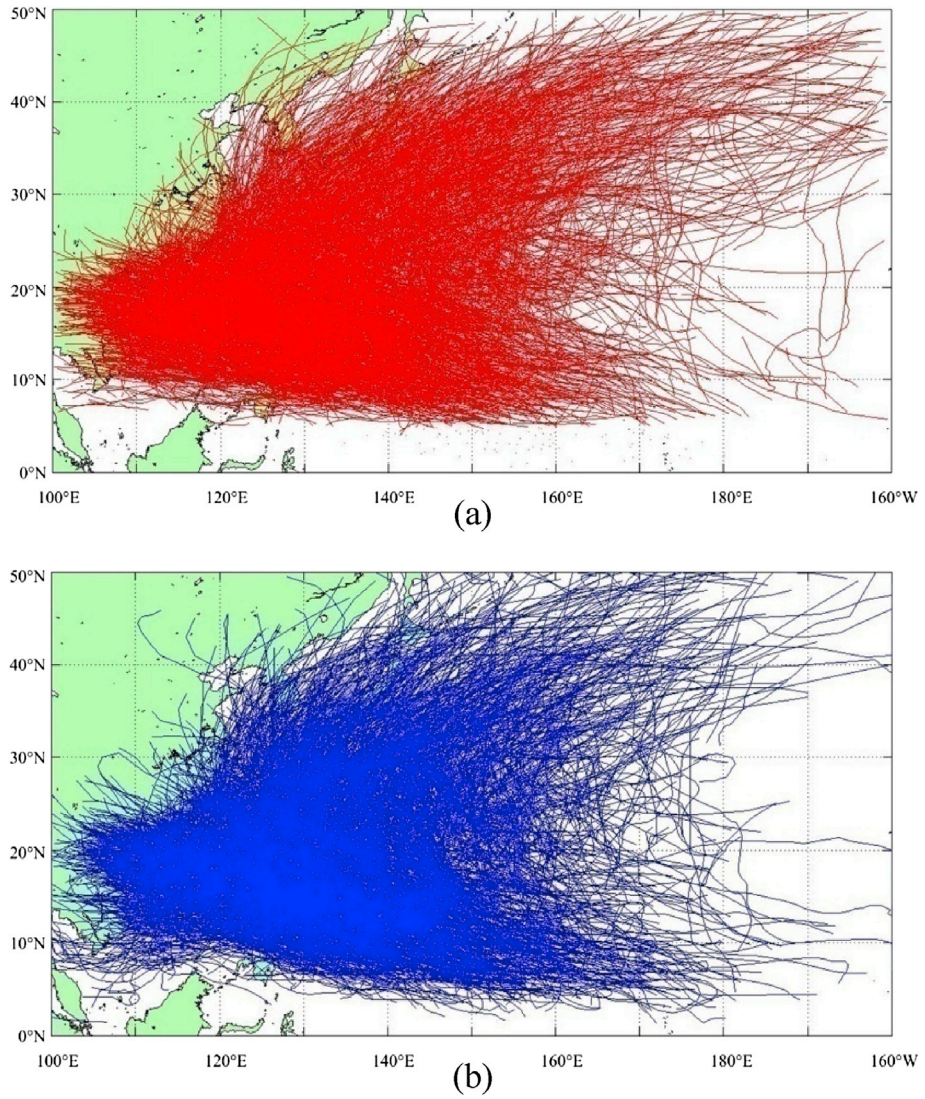

Fig. 6. Spatial distributions of the simulated 66 years tracks (a) and historical tracks (b) from 1949 to 2014.

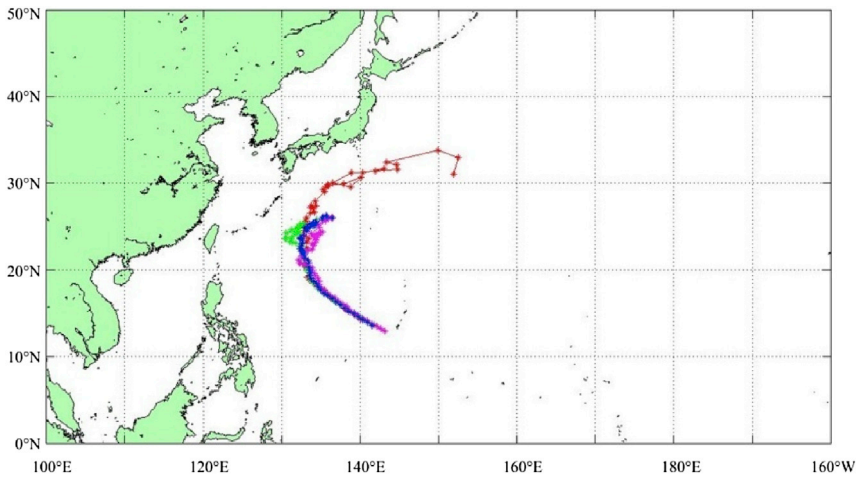

Fig. 7. Historical two-week average tracks in different two decades. The blue line is the overall average historical track of the period 1949–2014. The red line is the historical track averaged from the period 1949–1969. The green line is the historical track averaged from the period 1970–1990. The pink line is the historical track averaged from the period 1991–2011. The asterisk on the line represents every 6-h average position of track. (For interpretation of the references to colour in this figure legend, the reader is referred to the web version of this article.)

autoregressive equation is developed, as shown in Eq. (9b), for which the R-squared is 0.358 in the WNP basin.

$$\Delta(\ln I_2 - \ln I_1) = a_0 + a_1 \ln I_1 + a_2 SST_2 + a_3 V_{\max 1} + a_4 PI_2 + a_5 \Delta(SST_2 - SST_1) + a_6 \Delta(PI_2 - PI_1) \tag{9a}$$

$$\Delta(\ln I_{i+1} - \ln I_i) = b_0 + b_1 \ln I_i + b_2 \ln I_{i-1} + b_3 SST_{i-1} + b_4 V_{\max\, i-1} + b_5 PI_{i-1} + b_6 \Delta(SST_{i+1} - SST_i) + b_7 \Delta(SST_i - SST_{i-1}) + b_8 \Delta(V_{\max\, i} - V_{\max\, i-1}) + b_9 \Delta(PI_{i+1} - PI_i) + b_{10} \Delta(PI_i - PI_{i-1}) \tag{9b}$$

where a_0, b_0, etc., are the regional regression coefficients; i is the current moment; i+1 is the next 6-h moment; i-1 is the last 6-h moment; I is the relative intensity which is defined as V_{max}/PI; V_{max} is the maximum wind velocity; PI is the potential intensity described in Bister and Emanuel (2002), which is controlled by the sea surface temperature, the atmospheric ambient specific humidity and temperature; SST is the sea surface temperature. The regression coefficients of Eq. (9) are determined using the least squares method in each ocean grids as shown in section 3.2.

Since the TCs have effect on the environmental variables, the monthly mean atmospheric and oceanic environmental data are used in Eq. (9) and interpolated into the TC positions to remove the effect. The initial TC intensity is set to the lower limit of tropical storm intensity (17.2 m/s) in order to improve the early survival of TCs.

Once the simulated TCs move into the land, the decay model is used for estimating the inland intensities. The inland decay model described in Kaplan and DeMaria (2000) is established using an exponent function to estimate the decay of intensity over time. Slightly different from Eq. (3) given in Kaplan and DeMaria (2000), there is no reduction factor for the initial decay intensity term, because the intensity in the sea before landing is used for initial decay intensity here. The decay equation for inland intensity is illustrated in Eq. (10) as following.

$$MV = V_b + (V_{\max 0} - V_b)\exp(-\alpha T) \tag{10}$$

where V_{max0} is the initial intensity before landing; V_b is the background wind, assuming that the wind finally decays to a background wind rather than zero; α is the fitting parameter; T is the decay time starting from the first position before landing. In this decay model, V_b and α are evaluated using the k nearest historical inland positions. Silverman (1986) suggests the value of k is chosen to be $\sqrt{n}$ (n is the sample size of historical landing site) for maximum likelihood. The intensity model simulates the intensity

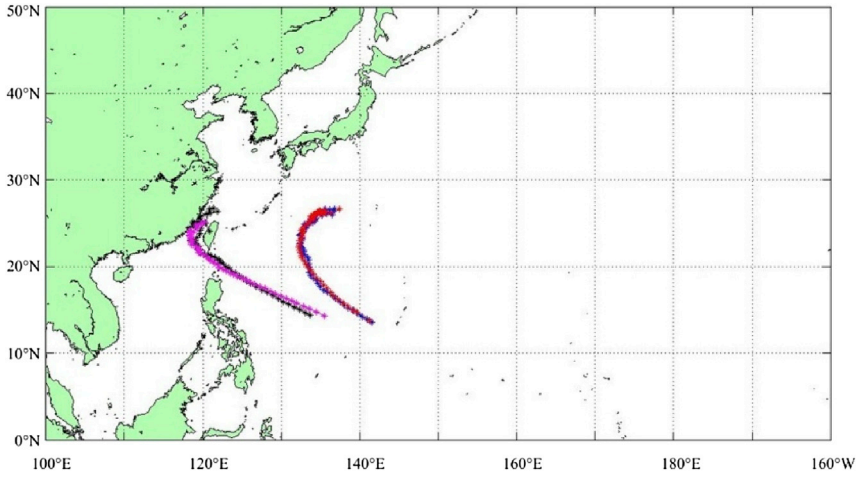

Fig. 8. Two-week average simulated track (red line) and two-week average historical track (blue line). Two-week average simulated track (pink line) and two-week average historical track (black line) for TCs landing China. (For interpretation of the references to colour in this figure legend, the reader is referred to the web version of this article.)

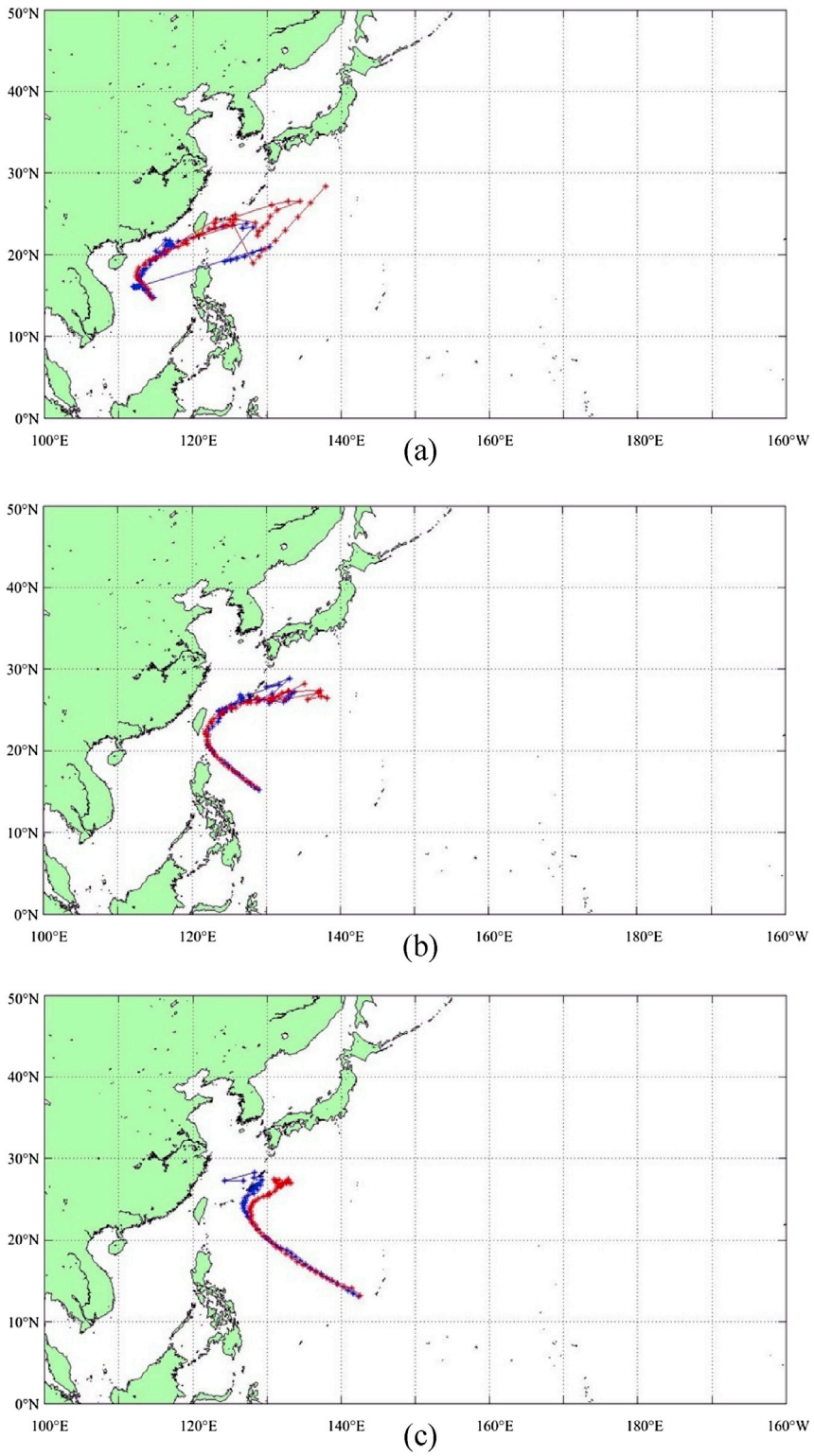

Fig. 9. Two weeks average simulated track (red line) and historical track (blue line) for initial genesis positions in four different longitude intervals. (a) 100°E–120°E; (b) 120°E–135°E; (c) 135°E–150°E; (d) 150°E–160°W. (For interpretation of the references to colour in this figure legend, the reader is referred to the web version of this article.)

until the intensity is lower than the minimum intensity of tropical depression (10.8 m/s), and then the full track model is terminated.

4. Model validation

Before simulating a full track, it should be noted that the original NCEP-NCAR reanalysis wind fields include the historical TC circulations. Thus the steering flow estimated directly from the original reanalysis wind fields may contain the contributions from the TC vortices. In order to eliminate the effect of TC vortices on steering flow, a filtering approach described in detail in Kurihara et al. (1995) is used to remove the historical TC vortices from the original wind fields. Here an example for filtering 850 hPa layer original wind field of typhoon Nuri at 0000UTC/19/08/2008 is shown in Fig. 5a. First, the original wind field

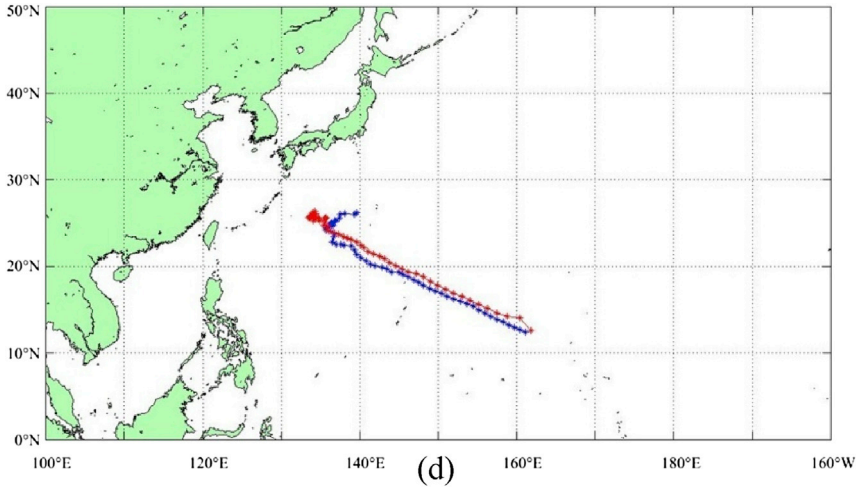

Fig. 9 (*continued*).

is filtered to obtain basic wind field through successive application of a smoothing operator, while the disturbance wind field is the deviation of the original field from the basic field. Second, an analyzed vortex domain, bounded by the red solid line shown in Fig. 5b, is determined and removed from the disturbance wind field depending on a certain boundary profile criteria of the disturbance wind speed. Third, the wind in the vortex-removed domain is interpolated by the outer wind field. Finally the environmental wind field is obtained by superimposing the basic field and the no-vortex disturbance filed.

A total of 28,136 full tracks for 1000 years are simulated through the improved full track model. Considering that presenting all simulated tracks in one figure would make it too crowded, Fig. 6 presents only 66 years of tracks that are extracted randomly from the 1000 simulated years and compared with the historical trajectories. Generally the spatial

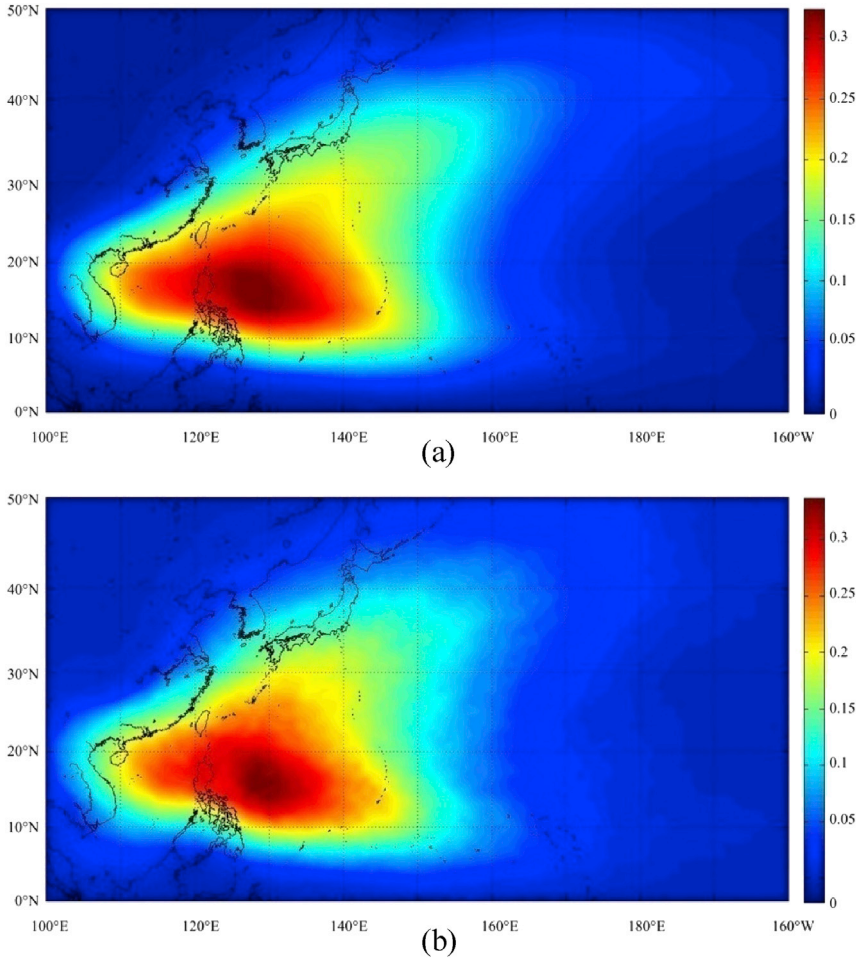

Fig. 10. Simulated (a) and historical (b) passing rate nephograms for individual positions within a 500 km radius.

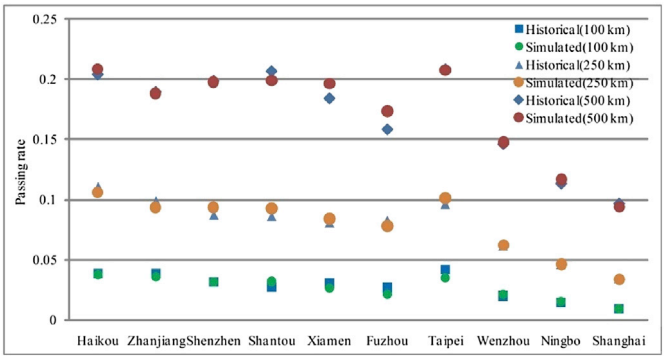

Fig. 11. Simulated and historical passing rates for 10 cities in the southeast China within 100, 250 and 500 km radii.

Table 1
Geographic coordinates for 10 cities along the coast of southeast China.

City	East longitude	North latitude
Haikou	110.35	20.02
Zhanjiang	110.35	21.22
Shenzhen	113.96	22.59
Shantou	116.73	23.36
Xiamen	118.37	24.53
Fuzhou	119.32	26.04
Taipei	121.56	25.09
Wenzhou	120.70	27.99
Ningbo	121.55	29.87
Shanghai	121.47	31.23

distribution of simulated tracks is in good agreement with that of the historical tracks. The simulated tracks mainly follow straight and recurving tracks, just as the historical tracks, which impact the southern and eastern parts of China respectively. It is noted that the simulated tracks are still insufficient in some regions. For example, the number of simulated tracks passing through the Japanese sea is slightly less compared to the historical tracks due to involving of high latitude weather system, which is not fully considered in current model.

In order to further appreciate the quality of the simulated tracks, the overall average historical track of the period 1949–2014 is compared with the average simulated track. As shown in Fig. 7, it has found that the historical two-week average tracks in the three two-decades change barely except the track averaged from 1949 to 1969. A likely explanation for the deviation in the historical track averaged from 1949 to 1969 is that the historical records of TCs are incomplete in the pre-satellite era.

Fig. 8 compares the two-week average simulated track with the historical track. Obviously, the average simulated track is in good agreement with the average historical one, which indicates our model successfully reproduces tracks based on the current atmosphere environment data in the WNP basin. For the TCs landing China, a comparison of two-week average simulated and historical tracks are also presented in Fig. 8. Clearly, the two-week average simulated track also coincides with the average historical track, showing that they move northwestward to southeast sea area of Taiwan, and then entwine due to the decay of landing. The ratios of the number of TCs landing China to the total number of TCs in the WNP are 0.243 and 0.244 for historical and simulated trajectories respectively. Apparently the difference is tiny.

Furthermore, Fig. 9 displays the two weeks average simulated and historical track for initial genesis positions in four different longitude intervals. Similarly, the average simulated tracks are consistent with average historical tracks for each generation position interval in their early to mid-phase; however, there is a significant deviation for the average tracks in the later stage. The reason may be in two folds: (1) the samples of historical tracks in the later stage are much fewer than that of the simulated tracks, and (2) the decay of historical TCs after landing is more complicate and different from that of simulated TCs.

The passing rate of a location is defined as the ratio of the number of TCs passing a defined radius to the total number of TCs, and used as an index for the TC hazard analyses. Fig. 10 shows the simulated and historical passing rates for individual positions within a 500 km radius. It can be seen that the high incidence areas are located in the Philippine Sea and the South China Sea, which is reflected by both the simulated and historical trajectories. Moreover, the nephogram of simulated passing rate is smoother than that of historical passing rate as the number of simulated tracks is 15 times the historical number. Although the passing rates of simulated tracks and historical tracks appear to be consistent in general, there exists difference in some regions, for example, the simulated passing rates in Korea and northern part of Japanese sea are slightly smaller compared to the historical passing rates, while the simulated rates in north of the South China Sea are slightly larger relative to the historical ones.

The coast of southeast China is the area most affected by TCs in China, which we are concerned. Therefore, the simulated passing rates for 10 cities in the southeast China within 100, 250, and 500 km radii are compared with that of historical records, as listed in Fig. 11. The 10 major cities spread along the coast of southeast China, and their geographic coordinates are given in Table 1. As seen in Fig. 11, the simulated results agree well with the historical statistics within 100 km and 250 km radii. For the passing rates within the 500 km radius, the simulated results are also consistent with the historical statistics except that the simulated passing rates at Xiamen and Fuzhou are slightly larger than historical passing rates within the 500 km radius.

Moreover, Figs. 12–15 show a comparison for the frequency distributions of four characteristics of the simulated and historical TCs for 10 cities in the southeast China within a 500 km radius. The four TC characteristics include translational speed, heading, minimum distance between TC center and target city, and intensity. The statistics of the simulated TC translation velocity, heading, and minimum distance agree well with that of the historical TCs. The simulated and historical cumulative frequency distributions of TC intensity in excess of 24.5 m/s in the southeast China are essentially in agreement, except for Shanghai, for which the simulated cumulative distribution overestimates the number of intense severe typhoon, noting that there are few historical TCs passing Shanghai. In general, the above comparisons suggest the adequacy of our track model in assessing typhoon wind risk in the coastal areas of southeast China.

5. Estimated typhoon wind hazard in the southeast China

5.1. Wind field model

To estimate the annual maximum typhoon wind velocity used for assessing typhoon wind hazard in the coastal areas of southeast China, the TCs passing a location within the 500 km radius are selected from the simulated track dataset. The positions and intensities of simulated TCs at every 10-min are interpolated using that of TCs at every six-hour. In this study, a gradient wind balance equation described in Georgiou (1985) is used to evaluate the gradient wind speed produced by the TCs shown in Eq. (11). The Georgiou's model assumes that the gradient wind field is determined by an axisymmetric parametric pressure field.

$$V(\alpha, r) = \frac{1}{2}(V_T \sin(\alpha) - fr) + \sqrt{\frac{1}{4}(V_T \sin(\alpha) - fr)^2 + \frac{B\Delta p}{\rho}\left(\frac{R_{\max}}{r}\right)^B \exp\left[-\left(\frac{R_{\max}}{r}\right)^B\right]} \tag{11}$$

where V_T is the translation speed; α is the clockwise angle from the storm moving direction; f is the Coriolis parameter of pending position; r is the distance from TC center; ρ is the air density; V is the gradient wind speed;

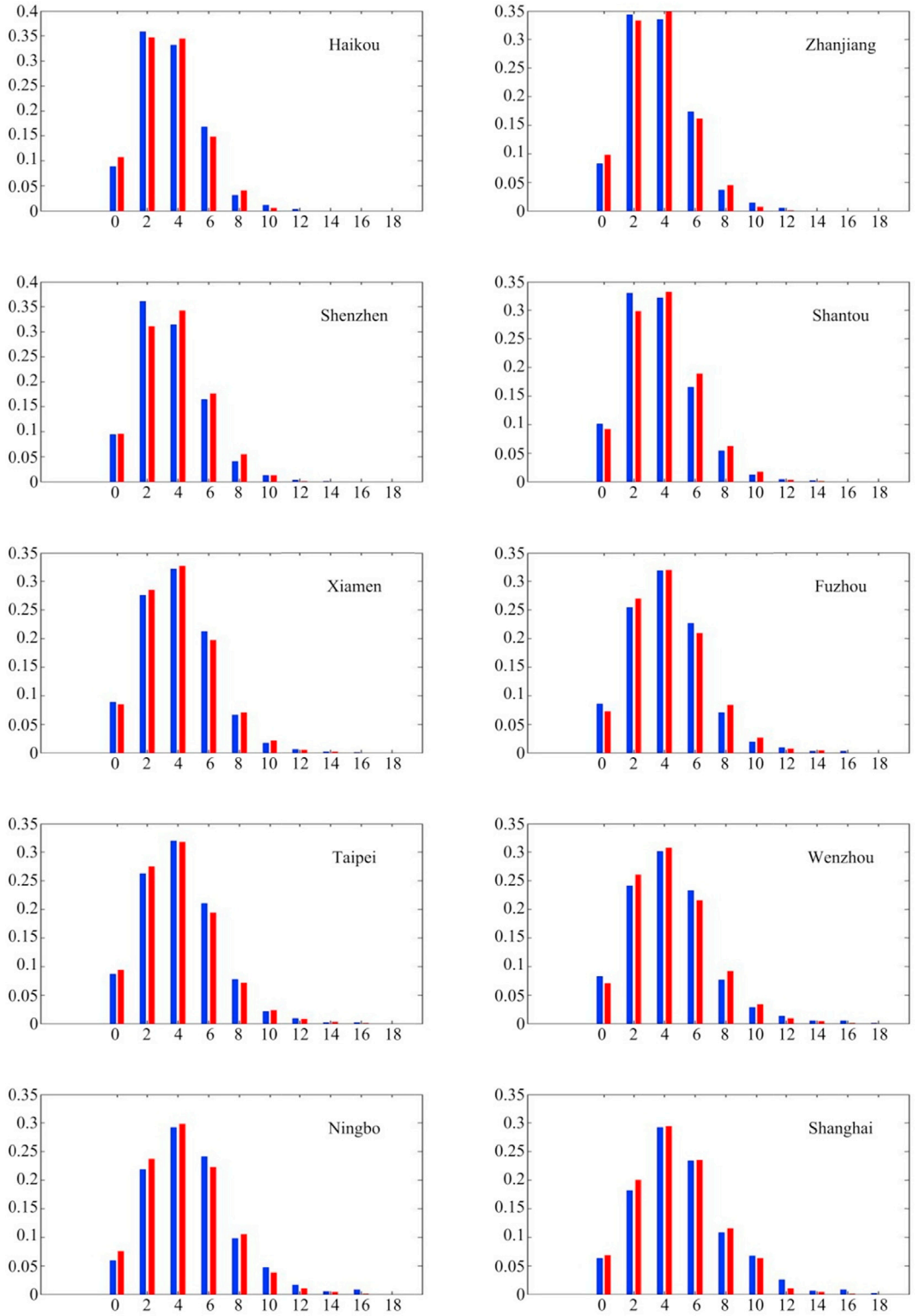

Fig. 12. Simulated and historical TC translational speed magnitude frequency distributions for 10 cities in the southeast China within a 500 km radius. The blue bars are historical frequency distributions. The red bars are simulated frequency distributions. The abscissa presents translational speed magnitude (unit: m/s) and the ordinate presents frequency distribution. (For interpretation of the references to colour in this figure legend, the reader is referred to the web version of this article.)

Δp is the center pressure deficit; $R_{\max}$ is the maximum wind speed radius; B is the Holland pressure profile parameter. Here B is determined by using Eq. (23) given in Vickery and Wadhera (2008), which is a function of maximum wind speed radius and Coriolis parameter.

$$B = 1.833 - 0.326\sqrt{f_c R_{\max}} \tag{12}$$

where f_c is the Coriolis parameter at the TC center. It is noteworthy that the simulated intensity in Eq. (9) is the maximum wind velocity at 10 m height instead of center pressure deficit. Therefore a regression equation relating the surface maximum wind speed to the central pressure deficit is established for ocean and land, of which the R-squared are 0.981 and 0.988 respectively.

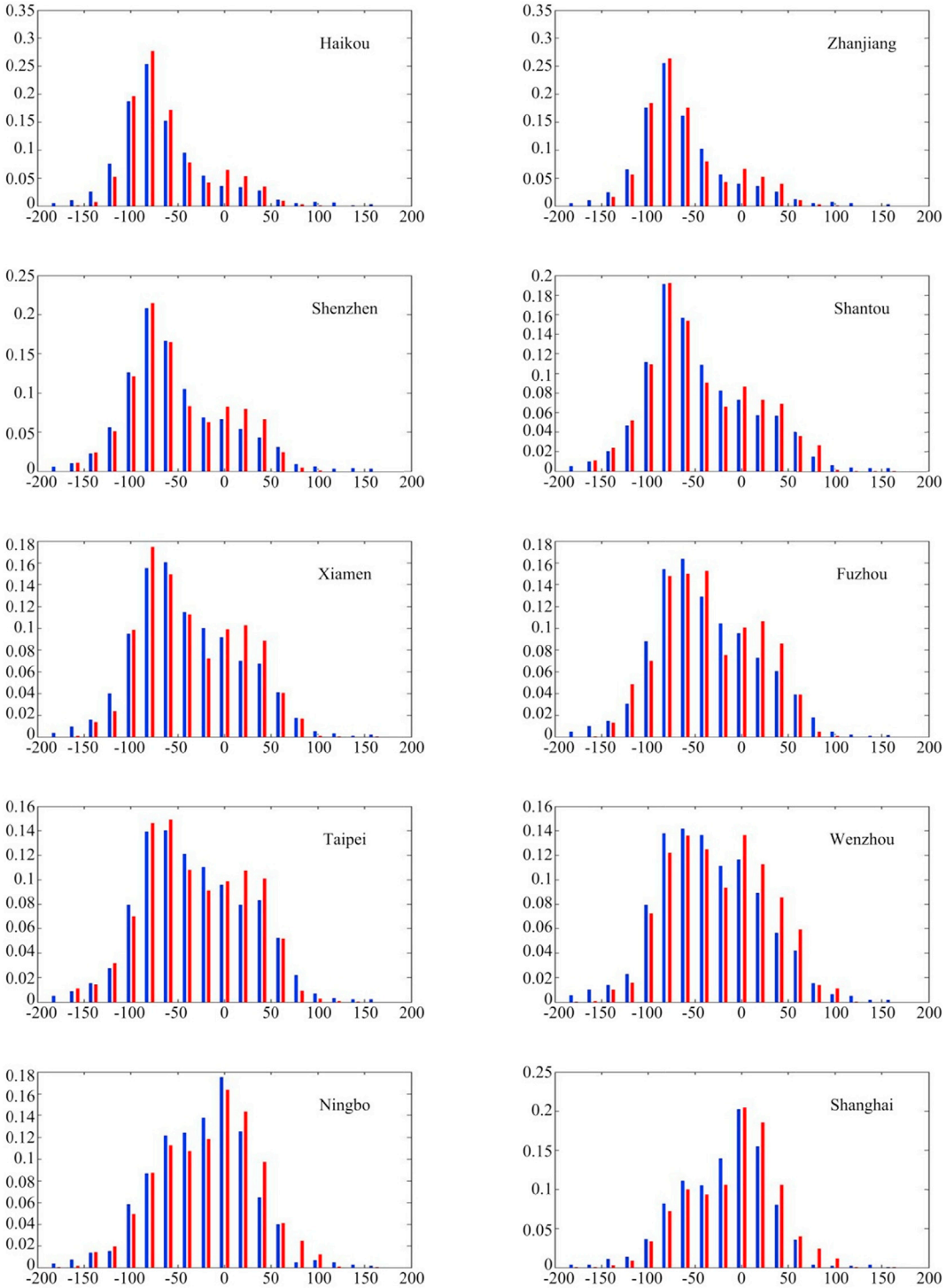

Fig. 13. Simulated and historical TC heading frequency distributions for 10 cities in the southeast China within a 500 km radius. 90° represents TC heading east and −90° represents TC heading west. The blue bars are historical frequency distributions. The red bars are simulated frequency distributions. The abscissa presents heading angle magnitude and the ordinate presents frequency distribution. (For interpretation of the references to colour in this figure legend, the reader is referred to the web version of this article.)

$$\Delta p_{\text{ocean}} = -0.954 + 0.387 V_{\max}^{1.313}, \text{ for ocean} \tag{13a}$$

$$\Delta p_{\text{land}} = -4.317 + 0.673 V_{\max}^{1.182}, \text{ for land} \tag{13b}$$

The coefficients in Eq. (13) are regressed using the JTWC best-track dataset selected for the TCs whose intensities are more than 17.2 m/s and the central pressure deficit is in units of hPa. Thus the simulated maximum wind velocity at 10 m height is translated into center pressure deficit, and then substituted into Eq. (11) to estimate the gradient wind field. The surface wind speed can be obtained through a gradient-to-surface wind speed conversion factor V_{10}/V_G. Vickery et al. (2009) revealed that V_{10}/V_G over the ocean varies from 0.67 to 0.74, while the reduction of V_{10}/V_G in the sea-to-land transition is in the range of 18–20% at the coast, and 23–28% for 50 km inland. For the sake of simplicity, V_{10}/V_G is set to 0.71 over the ocean and reduces by 19% at the coast, and 25% for 50 km inland.

In order to further validate the adequacy of the above wind field model, a simulation for typhoon Hagupit (2008) is performed by solving

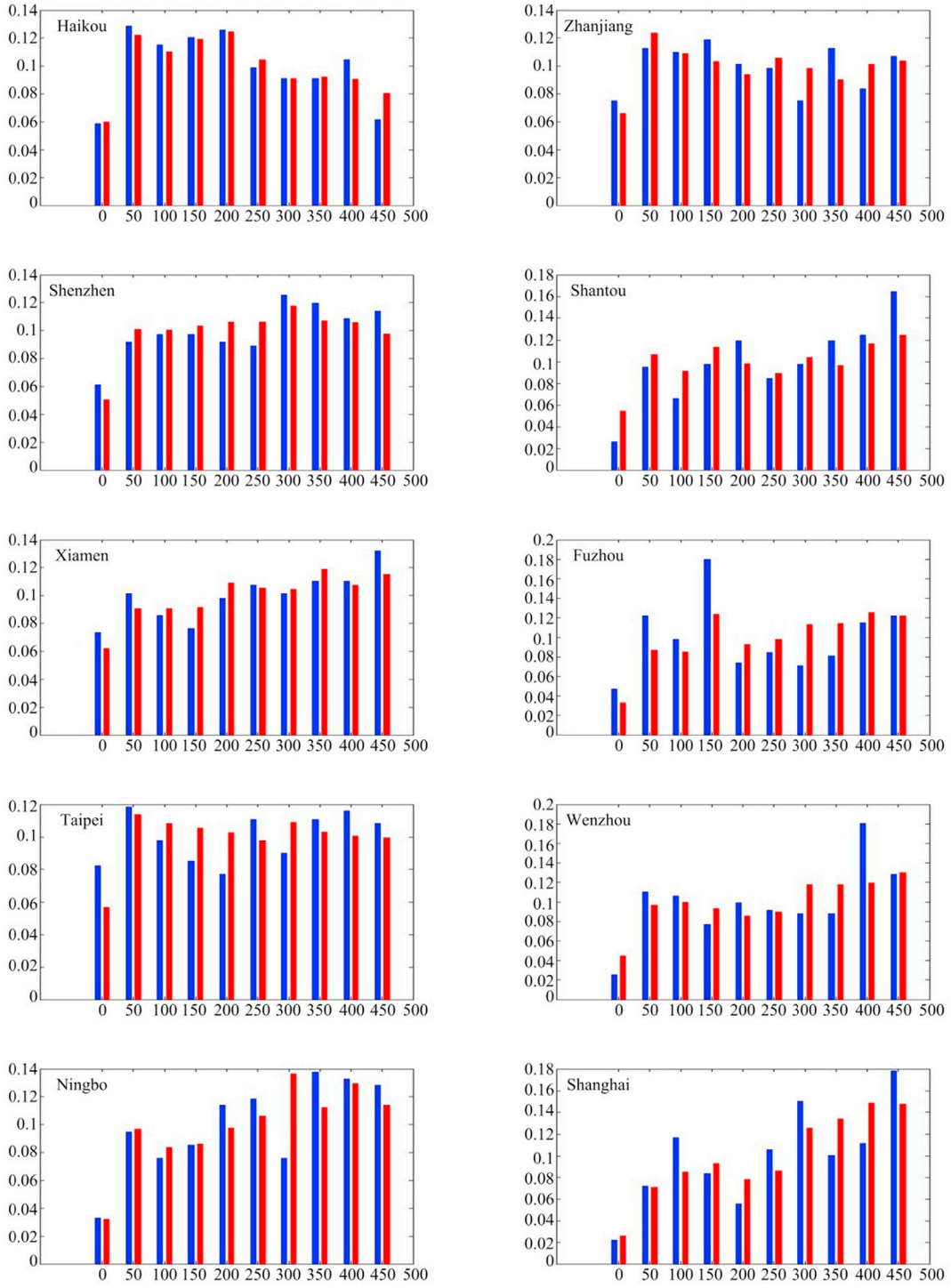

Fig. 14. Simulated and historical frequency distributions of minimum distance between TC center and city for 10 cities in the southeast China within a 500 km radius. The blue bars are historical frequency distributions. The red bars are simulated frequency distributions. The abscissa presents distance magnitude (unit: km) and the ordinate presents frequency distribution. (For interpretation of the references to colour in this figure legend, the reader is referred to the web version of this article.)

Eqs. (11)-(13) using the JTWC best track information, and compared with the measured surface wind speeds at two different meteorological stations. The simulated and measured hourly mean wind speed histories of typhoon Hagupit at two meteorological stations are shown in Fig. 16. It can be seen that the simulated results are consistent with the observed ones in general. The relative errors between the simulated and measured maximum wind speed are both less than 5% at two selected sites.

5.2. Estimated maximum wind for return period of 50 and 100 years in the southeast China

In Georgiou's model, the maximum wind speed radius is a key parameter to control the gradient wind speed. Therefore, the maximum wind speed radii of historical records with more than 17.2 m/s wind speed are selected for developing a regressive model of maximum wind speed radius based on the maximum wind and TC position, as shown in Eq. (14).

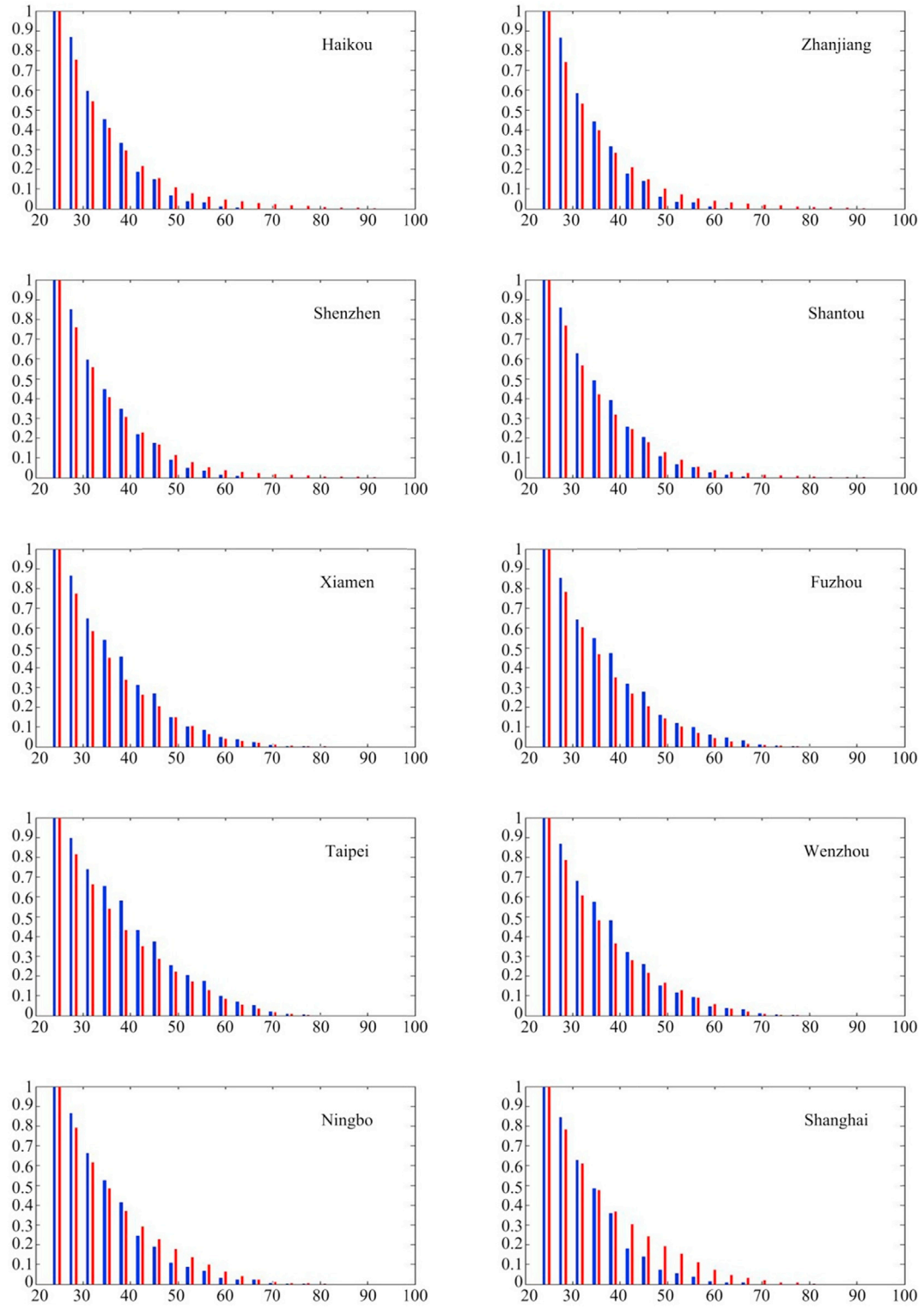

Fig. 15. Simulated and historical cumulative frequency distributions of TC intensity in excess of 24.5 m/s for 10 cities in the southeast China within a 500 km radius. The blue bars are historical frequency distributions. The red bars are simulated frequency distributions. The abscissa presents TC intensity magnitude (unit: m/s) and the ordinate presents frequency distribution. (For interpretation of the references to colour in this figure legend, the reader is referred to the web version of this article.)

$$\ln R_{\max} = a_0 + a_1 \ln V_{\max} + a_2 lon + a_3 lat + \varepsilon \quad (14)$$

where *lon* and *lat* are the longitude and the latitude of TC center respectively; ε is modeled as Gaussian noise with N(0, σ^2); the maximum wind speed radius is in unit of km. The regressive coefficients estimated for the 10 cities using historical records within a 500 km radius of each city are listed in Table 2.

Using Eqs. (11)-(14), the gradient wind speeds of 10 cities produced by the simulated TCs are estimated and converted to surface wind speeds at 10 m height. The annual maximum typhoon wind velocities are picked out for estimating 50-year and 100-year return period values of maximum speed (short for V_{50} and V_{100}).

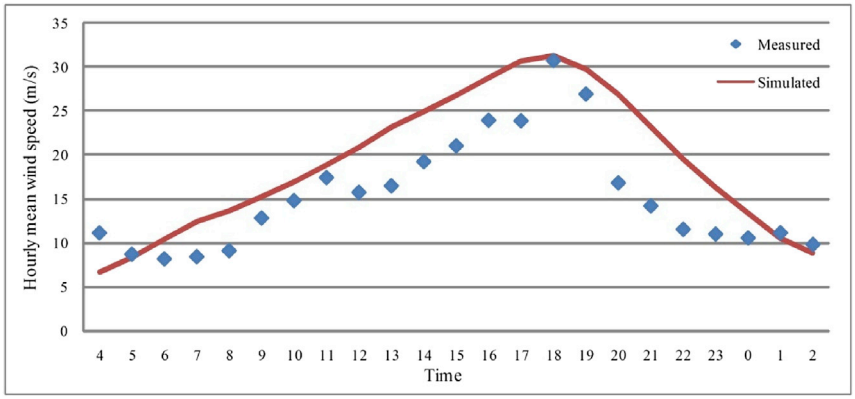

(a) Shangchuandao station (Start from 0400UTC/23/09/2008)

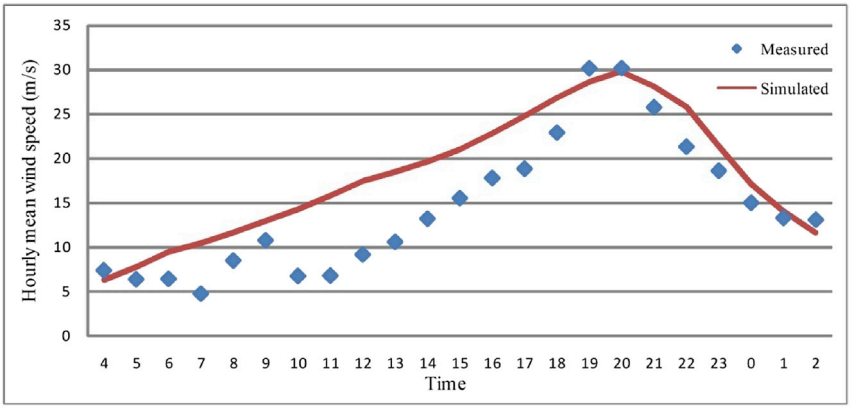

(b) Yangjiang station (Start from 0400UTC/23/09/2008)

Fig. 16. Comparison of simulated and measured hourly mean wind speed histories of typhoon Hagupit (2008) at two meteorological stations; (a) Shangchuandao site (112.77E, 21.73N) and (b) Yangjiang (111.97E, 21.83N). The two meteorological stations are both located in open terrain near the coast.

As shown in Table 3, the estimated V_{50} and V_{100} are compared with those recommended in Chinese design code (GB 50009–2012). The estimated V_{50} and V_{100} in all 10 cities vary widely along the coast of southeast China. The estimated V_{50} and V_{100} at Wenzhou and Ningbo are comparable to that of Shenzhen and Shantou, indicating that Wenzhou and Ningbo will encounter few but intense typhoons. The largest deviation between the maximum wind speed V_{50} estimated by our model and those recommended in design code occurs in Ningbo, where the modeled speed is 13.4% higher than the code recommended speed. To the author's knowledge, the wind records used and the procedures employed in the development of the design wind speeds in current Chinese code are not documented in literature that are publicly available, the discrepancy shown in Table 3 is not un-usual and deserves further exploration.

6. Conclusions

The paper proposed an improved full track model for TCs based on statistical dynamics method to extend the TC dataset for assessing the typhoon wind hazard in the coast of southeast China. The improved model inherits the idea of synthetic full track, but distinguishes itself from previous empirical full track model. The model combines with the environment data to simulate TC tracks based on the statistical dynamics relationship of TC instead of simply statistical characteristics of historical tracks.

This study focuses on improving the genesis, track and intensity simulation of TCs based on a more solid meteorological basis. Different from the traditional method extracting directly historical genesis

Table 2
Regressive model parameters of maximum wind speed radius in 10 cities, including the regression coefficients a_0, a_1, a_2, variance σ^2, and R-squared r^2.

City	a_0	a_1	a_2	a_3	σ^2	r^2
Haikou	5.930	−0.764	0.005	−0.006	0.121	0.361
Zhanjiang	6.561	−0.679	0.002	−0.038	0.106	0.341
Shenzhen	4.577	−0.842	0.022	−0.022	0.157	0.365
Shantou	3.593	−0.846	0.030	−0.021	0.179	0.309
Xiamen	5.177	−0.871	0.015	−0.007	0.142	0.392
Fuzhou	4.512	−0.916	0.021	−0.004	0.138	0.440
Taipei	4.298	−0.857	0.022	−0.010	0.133	0.448
Wenzhou	5.248	−0.792	0.009	0.008	0.156	0.360
Ningbo	6.354	−0.941	−0.004	0.041	0.129	0.515
Shanghai	4.797	−1.028	0.018	0.013	0.128	0.523

Table 3
50-year and 100-year return period maximum wind speeds (units: m/s) for 10 cities.

City	V_{50}		V_{100}	
	GB 50009-2012	The synthesized full track method	GB 50009-2012	The synthesized full track method
Haikou	34.6	36.4	37.9	38.5
Zhanjiang	35.8	34.2	39.0	37.5
Shenzhen	34.6	32.8	37.9	36.4
Shantou	35.8	33.9	39.0	37.3
Xiamen	35.8	34.5	39.0	37.7
Fuzhou	33.5	30.1	36.9	33.6
Taipei	33.5	35.9	36.9	37.6
Wenzhou	31.0	32.5	33.5	34.9
Ningbo	28.3	32.1	31.0	34.5
Shanghai	29.7	29.6	31.0	31.7

positions, a genesis probability model is developed based upon an improved kernel probability density function with the best bandwidths estimated by biased cross-validation method. The movement model is established using the BAM, including steering flow model and beta drift model. The steering flow is defined as a 300 to 850 hpa pressure-weighted mean wind averaged over annulus 5° latitude from the TC center and the beta drift is estimated by regional mean beta-drift velocity. The intensity model consists of an ocean intensity model and an inland decay model; the former is established based on an auto-regression model of maximum wind speed through the stepwise regression method, while the latter is fitted as a decreasing exponential function through selecting the k nearest landing positions.

A total of 28,136 full tracks for 1000 years are simulated using the atmosphere and ocean environmental data, of which all historical TC vortices are removed. Generally, the spatial distribution of simulated tracks is in good agreement with that of the historical tracks. Despite some slight bias at some locations, our model generally performs well by comparing the spatial track distributions, the average tracks, and passing rates of simulated tracks with that of the historical records in the WNP basin. Furthermore, a comparison of four characteristic frequency distributions of the simulated and historical TCs for 10 cities in the southeast China is performed to check the adequacy of our track model's performance in the coast of southeast China. On the whole, these comparisons suggest the adequacy of the improved track model in assessing TC risk in the coastal area of southeast China.

Moreover, the improved full track model is combined with a parametric wind field model to estimate annual maximum wind velocities for return period of 50 and 100 years, which indicates the estimated V_{50} and V_{100} in all 10 cities vary widely along the coast of southeast China. Compared with those recommended in Chinese design code (GB 50009–2012), the largest deviation of return period velocity occurs in Ningbo, the difference is not un-usual and deserves further exploration. In the future, the improved full track model will be combined with the future environmental data provided by general circulation models to simulate more highly resolved future TC events, assessing the impact of climate change on TC hazard in the coast of southeast China.

Acknowledgments

The first author is grateful to Prof. Kerry A. Emanuel from Massachusetts Institute of Technology for providing his simulated tracks through a statistical deterministic approach. The authors are also grateful to Prof. H. P. Hong from University of Western Ontario for his helpful critique of the wind hazard analyses. Financial support from the Natural Science Foundation of China [grant numbers 91215302, 51378155] is gratefully acknowledged.

References

Batts, M.E., Simiu, E., Russell, L.R., 1980. Hurricane wind speeds in the United States. J. Struct. Div. 106 (10), 2001–2016.

Bister, M., Emanuel, K.A., 2002. Low frequency variability of tropical cyclone potential intensity-1. Interannual to interdecadal variability. J. Geophys. Res. Atmos. 107D24, 4801. https://doi.org/10.1029/2001JD000776.

Carr, L.E., Elsberry, R.L., 1990. Observational evidence for predictions of tropical cyclone propagation relative to environmental steering. J. Atmos. Sci. 47 (4), 542–546. https://doi.org/10.1175/1520-0469%281990%29047%3c0542:OEFPOT%3e2.0.CO%3b2.

Chan, J.C.L., 2005. The physics of tropical cyclone motion. Annu. Rev. Fluid Mech. 37, 99–128. https://doi.org/10.1146/annurev.fluid.37.061903.175702.

Colbert, A.J., Soden, B.J., Vecchi, G.A., Kirtman, B.P., 2013. The impact of anthropogenic climate change on north Atlantic tropical cyclone tracks. J. Clim. 26 (12), 4088–4095. https://doi.org/10.1175/JCLI-D-12-00342.1.

Emanuel, K., Ravela, S., Vivant, E., 2006. A statistical deterministic approach to hurricane risk assessment. Bull. Amer. Meteor. Soc. 87 (3), 299–314. https://doi.org/10.1175/BAMS-87-3-299.

Emanuel, K., Sundararajan, R., Williams, J., 2008. Hurricanes and global warming - results from downscaling IPCC AR4 simulations. Bull. Amer. Meteor. Soc. 89 (3), 347–367. https://doi.org/10.1175/BAMS-89-3-347.

Emanuel, K., 2013. Downscaling CMIP5 climate models shows increased tropical cyclone activity over the 21st century. Proc. Natl. Acad. Sci. U. S. A. 110 (30), 12219–12224. https://doi.org/10.1073/pnas.1301293110.

Georgiou, P.N., 1985. Design Wind Speeds in Tropical Cyclone-prone Regions. PhD thesis. The University of Western Ontario. http://ir.lib.uwo.ca/digitizedtheses/1523.

Hall, T.M., Jewson, S., 2007. Statistical modelling of North Atlantic tropical cyclone tracks. Tellus 59A, 486–498. https://doi.org/10.1111/j.1600-0870.2007.00240.x.

Ishii, M., Shouji, A., Sugimoto, S., Matsumoto, T., 2005. Objective analyses of sea-surface temperature and marine meteorological variables for the 20th century using icoads and the Kobe collection. Int. J. Climatol. 25 (7), 865–879. https://doi.org/10.1002/joc.1169.

James, M.K., Mason, L.B., 2005. Synthetic tropical cyclone database. J. Waterw. Port. Coast. Ocean. Eng. 131 (4), 181–192. https://doi.org/10.1061/(ASCE)0733-950X(2005)131:4(181).

Kalnay, E., Kanamitsu, M., Kistler, R., 1996. The NCEP/NCAR 40-year reanalysis project. Bull. Amer. Meteor. Soc. 77 (3), 437–471. https://doi.org/10.1175/1520-0477%281996%29077%3c0437:TNYRP%3e2.0.CO%3b2.

Kaplan, J., DeMaria, M., 2000. On the decay of tropical cyclone winds after landfall in the New England area. J. App. Meteor 40 (2), 280–286. https://doi.org/10.1175/1520-0450%282001%29040%3c0280:OTDOTC%3e2.0.CO%3b2.

Kurihara, Y., Bender, M.A., Tuleya, R.E., 1995. Improvements in the GFDL hurricane prediction system. Mon. Weather. Rev. 123 (9), 2791–2801. https://doi.org/10.1175/1520-0493%281995%29123%3c2791:IITGHP%3e2.0.CO%3b2.

Li, S.H., Hong, H.P., 2016. Typhoon wind hazard estimation for China using an empirical track model. Nat. Hazards 82 (2), 1009–1029. https://doi.org/10.1007/s11069-016-2231-2.

Marks, D.G., 1992. The beta and advection model for hurricane track forecasting. NOAA Tech. Memo. NWS NMC 70, 89 pp. https://repository.library.noaa.gov/view/noaa/7184.

Russell, L.R., 1971. Probability distributions for hurricane effects. J. Waterw. Harb. Coast. Eng. Div. Amer. Soc. Civ. Eng. 97, 139–154.

Sain, S.R., Baggerly, K.A., Scott, D.W., 1994. Cross-validation of multivariate densities. J. Amer. Stat. Asso 89 (427), 807–817. https://doi.org/10.1080/01621459.1994.10476814.

Scott, D.W., 2012. Multivariate Density Estimation Theory Practice and Visualization, second ed. Wiley, New Jersey.

Silverman, B.W., 1986. Density Estimation for Statistics and Data Analysis, first ed. Chapman & Hall, London.

Terrell, G.R., Scott, D.W., 1992. Variable kernel density estimation. Ann. Stat. 20 (3), 1236–1265.

Tryggvason, B.V., Surry, D., Davenport, A.G., 1976. Predicting wind-induced response in hurricane ones. J. Struct. Div. 102 (12), 2333–2350.

Vickery, P.J., Twisdale, L.A., 1995. Wind-field and filling models for hurricane wind-speed predictions. J. Struct. Eng. 121 (11), 1700–1709. https://doi.org/10.1061/(ASCE)0733-9445(1995)121:11(1700).

Vickery, P.J., Skerlj, P.F., Twisdale, L.A., 2000. Simulation of hurricane risk in the US using empirical track model. J. Struct. Eng. 126 (10), 1222–1237. https://doi.org/10.1061/(ASCE)0733-9445(2000)126:10(1222).

Vickery, P.J., Wadhera, D., 2008. Statistical models of Holland pressure profile parameter and radius to maximum winds of hurricanes from flight-level pressure and H*wind data. J. Appl. Meteorol. Climatol. 47 (10), 2497–2517. https://doi.org/10.1175/2008JAMC1837.1.

Vickery, P.J., Masters, F.J., Powell, M.D., Wadhera, D., 2009. Hurricane hazard modeling: the past, present, and future. J. Wind Eng. Ind. Aerodyn. 97 (7–8), 392–405. https://doi.org/10.1016/j.jweia.2009.05.005.

Vickery, P.J., Wadhera, D., Stear, J.D., 2010. SS Metocean/A Synthetic Model for Gulf of Mexico Hurricanes. Offshore Technology Conference, Houston, Texas.